Instability of Ga-substituted $Li_7La_3Zr_2O_{12}$ toward Metallic Li (supplementary)

Chih−Long Tsai[a,], Ngoc Thanh Thuy Tran [b], Roland Schierholz[a], Zigeng Liu[a], Anna Windmüller[a], Che-an Lin[c], Qi Xu[a,d], Xin Lu[a,d], Shicheng Yu[a], Hermann Tempel[a], Hans Kungl[a], Shih-Kang Lin[b,c,e], and Rüdiger–A. Eichel[a,d,f]*

[a]*Institut für Energie– und Klimaforschung (IEK–9: Grundlagen der Elektrochemie), Forschungszentrum Jülich, D–52425 Jülich, Germany*

[b]*Hierarchical Green-Energy Materials (Hi-GEM) Research Center, National Cheng Kung University, Tainan70101, Taiwan*

[c]*Department of Materials Science and Engineering, National Cheng Kung University, Tainan70101, Taiwan*

[d]*Institut für Materialien und Prozesse für elektrochemische Energiespeicher– und wandler, RWTH Aachen University, D–52074 Aachen, Germany*

[e]*Program on Smart and Sustainable Manufacturing, Academy of Innovative Semiconductor and Sustainable Manufacturing, National Cheng Kung University, Tainan70101, Taiwan*

[f]*Institut für Energie– und Klimaforschung (IEK–12: Helmholtz–Institute Münster, Ionics in Energy Storage), Forschungszentrum Jülich, D–48149 Münster, Germany*

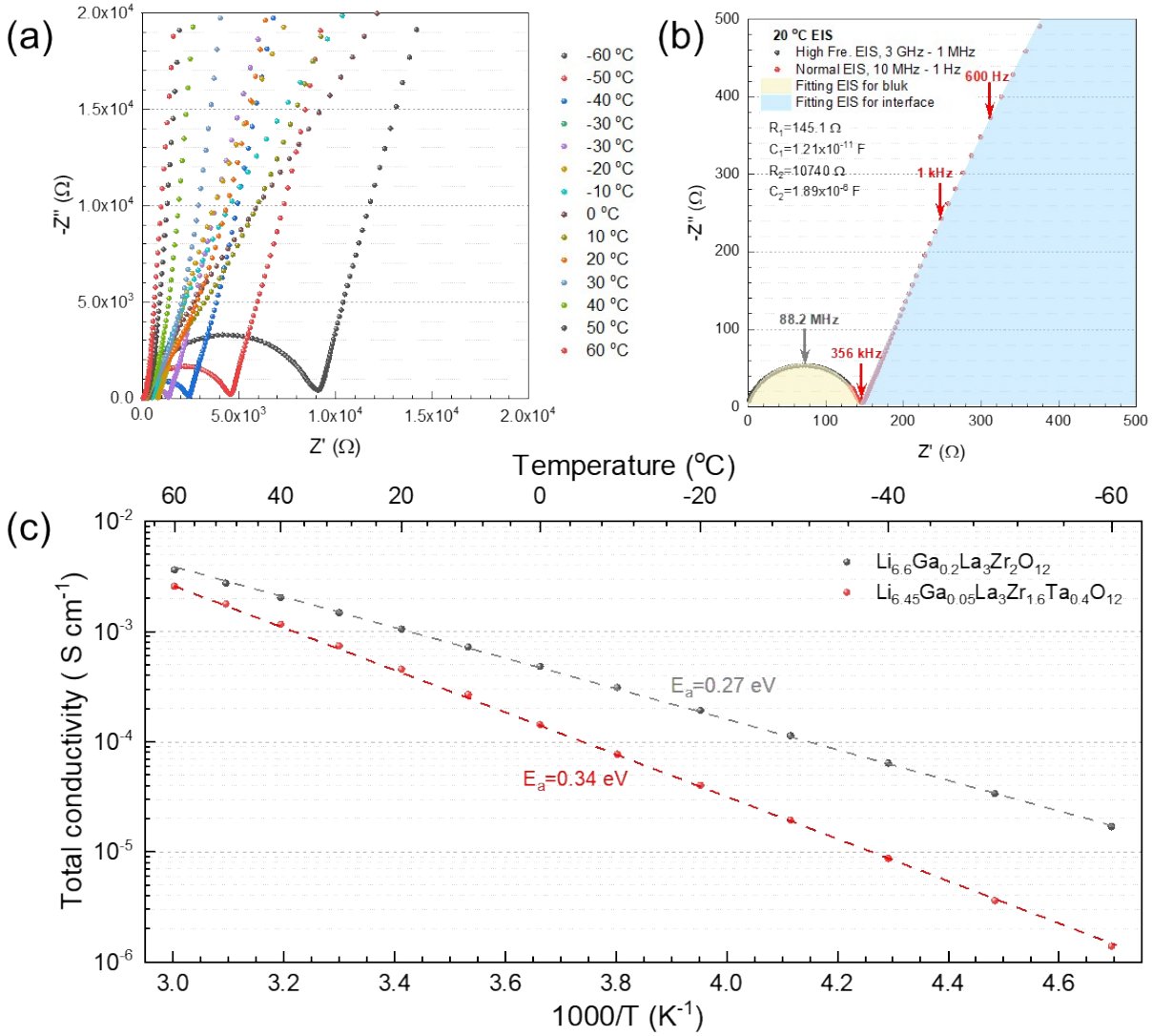

Figure S1. (a) Temperature dependent and (b) high frequency EIS Nyquist plots for $Li_{6.4}Ga_{0.2}La_3Zr_2O_{12}$. The high frequency EIS was measured from 3 GHz to 1 Hz at 20 °C. (c) Arrhenius plot of total conductivities for $Li_{6.4}Ga_{0.2}La_3Zr_2O_{12}$ and $Li_{6.45}Ga_{0.05}La_3Zr_{1.6}Ta_{0.4}O_{12}$. For the sake of readability, total conductivity vs. 1000/T is shown. The activation energies given in the figure were calculated from fitting Arrhenius equation.

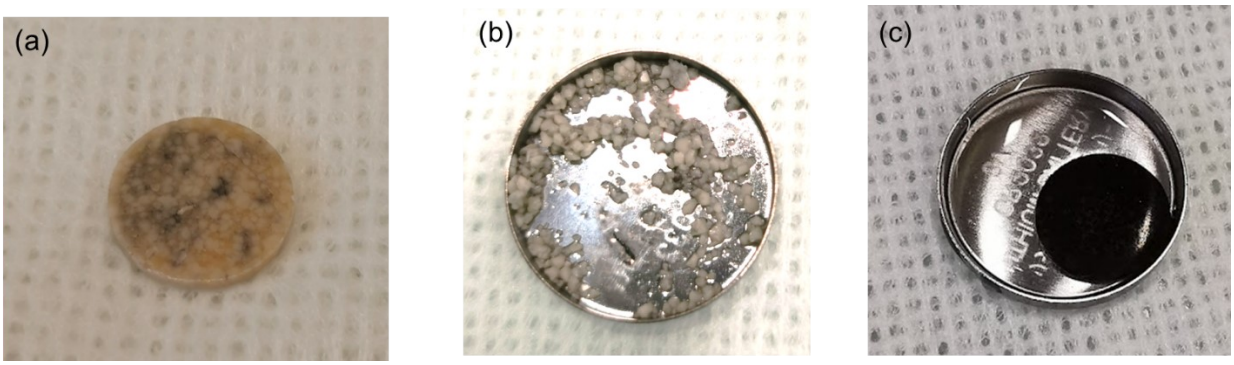

Figure S2. (a) $Li_{6.4}Ga_{0.2}La_3Zr_2O_{12}$ pellet get directly reduced by Li after isostatic press. Li electrodes were removed to see the surface of the pellet. (b) (reduced) $Li_{6.4}Ga_{0.2}La_3Zr_2O_{12}$ single crystals after the clean out of black color material using absolute ethanol. (c) reduced $Li_{6.45}Ga_{0.05}La_3Zr_{1.6}Ta_{0.4}O_{12}$ pellet in water. The pellet still holds the sintered body instead of falling apart.

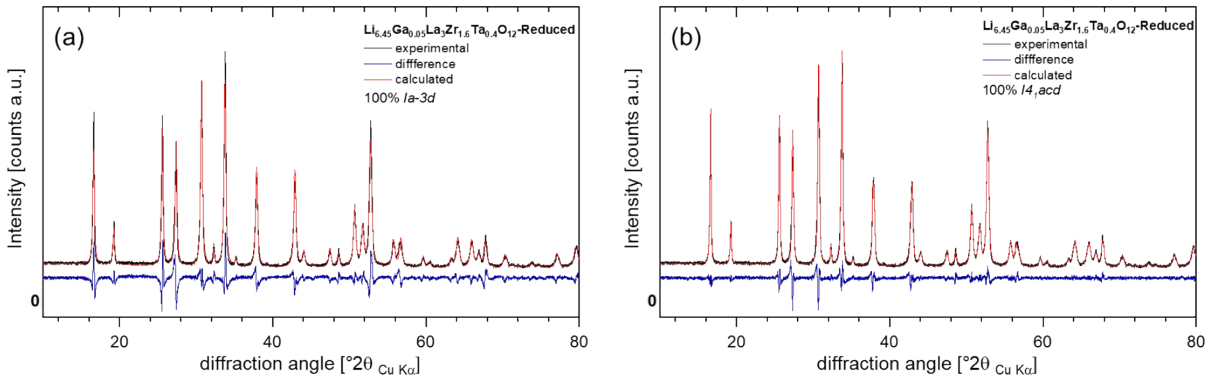

Figure S3. Refinement of reduced $Li_{6.45}Ga_{0.05}La_3Zr_{1.6}Ta_{0.4}O_{12}$ XRD pattern. (a) Fitting with cubic *Ia-3d* garnet while refining the parameter for line broadening left significant intensity contribution unfitted. (b) A more reasonable fit was achieved with the tetragonal phase $I4_1acd$.

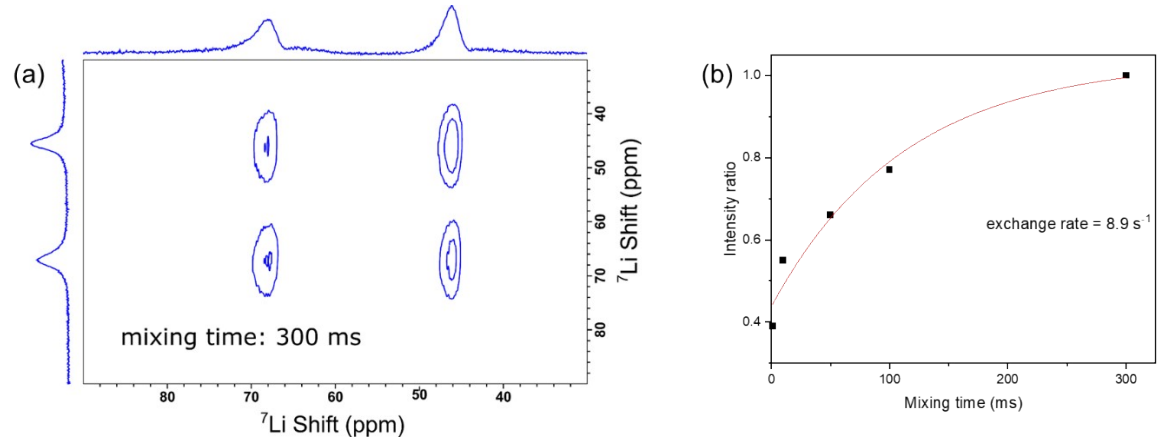

Figure S4. (A) 2D ^{7}Li–^{7}Li EXSY NMR spectrum of reduced $Li_{6.4}Ga_{0.2}La_3Zr_2O_{12}$; (B) corresponding chemical exchange build-up curves.

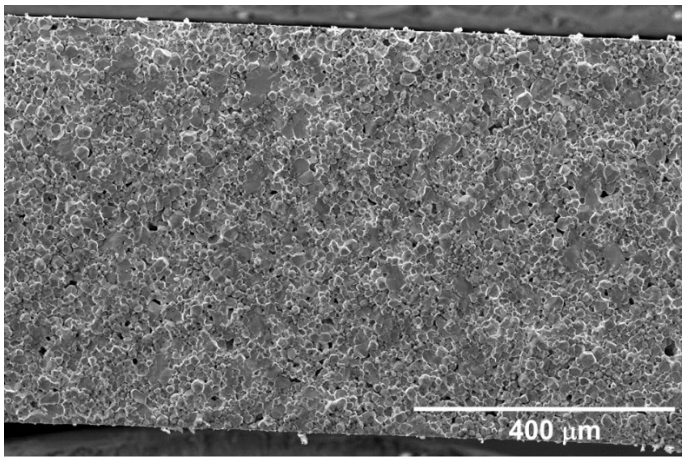

Figure S5. Microstructure of $Li_{6.45}Al_{0.05}La_3Zr_{1.6}Ta_{0.4}O_{12}$. The grain size is much homogeneous than $Li_{6.45}Ga_{0.05}La_3Zr_{1.6}Ta_{0.4}O_{12}$, which has large grain size as big as 500 μm.

To clarify the role of $LiGaO_2$ at the grain boundary, a pure phase $LiGaO_2$ was synthesized for the stability test again metallic Li, figure S6. Here, two methods were used for the stability test, one by attaching $LiGaO_2$ to Li foil at room temperature and the other by placing $LiGaO_2$ pellet onto a 250 °C heating plate after attaching Li foil onto it surface, figure S6(b) and movie S2. No noticeable reaction or changing of colour for both Li foil and $LiGaO_2$ sample at room temperature even after two weeks of storage in glove box. For the sample placing onto a 250 °C heating plate,

it can be seen from the video that $LiGaO_2$ fractured into small pieces when the temperature reaching Li melting point, indicating by the small piece of Li in the coin cell at the first 2 seconds of video. Before the melting point of Li, no noticeable reaction was observed. After the experiment, only the texture of metallic Li was changed but not $LiGaO_2$. The fracture of $LiGaO_2$ pellet at Li melting temperature and the change of metallic Li texture indicate that a reaction was ongoing between $LiGaO_2$ and Li at this temperature, which could be $(x+1)Li + LiGaO_2 \rightarrow Li_xGa + 2Li_2O$.

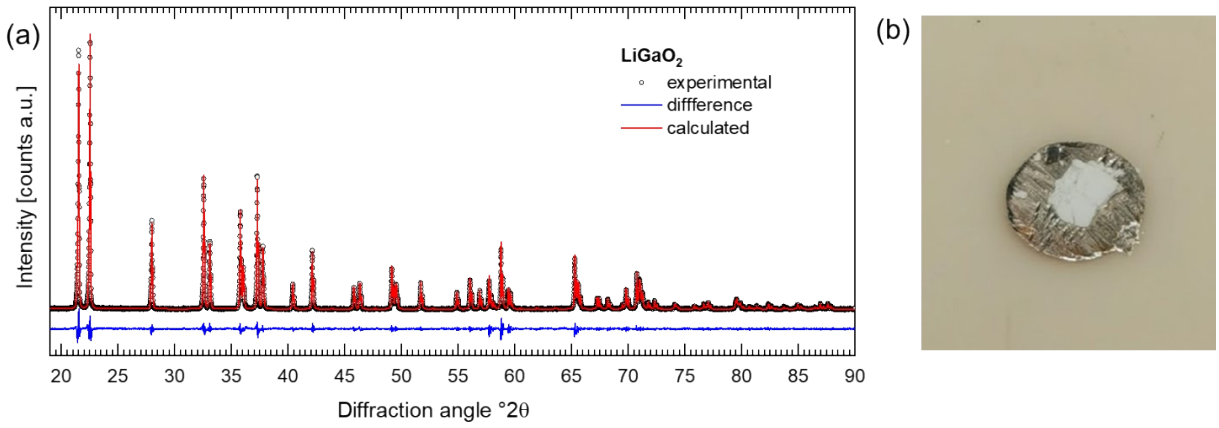

Figure S6. (a) XRD refinement for synthesized single phase $LiGaO_2$. (b) $LiGaO_2$ do not show any noticeable reaction when in contact with Li. The sample remains the same even after 30 days in a glove box.

Table S1. Calculated formation energies (E_f) of relevant compounds of Li-La-Zr-O-Ga at 0 K.

Compound	Space group	E_f (eV/atom)
$Li_7La_3Zr_2O_{12}$	$Ia\bar{3}d$	-3.184
$Li_{6.625}Ga_{0.125}La_3Zr_2O_{12}$	$Ia\bar{3}d$	-3.185
$Li_{6.25}Ga_{0.25}La_3Zr_2O_{12}$	$Ia\bar{3}d$	-3.194
$Li_{7.25}La_3Zr_2O_{12}$	$Ia\bar{3}d$	-3.145
$Li_{7.375}La_3Zr_2O_{12}$	$Ia\bar{3}d$	-3.124
$Li_{7.5}La_3Zr_2O_{12}$	$Ia\bar{3}d$	-3.106
Zr_3O	R32	-1.581

Zr_2O	P312	-2.013
Zr_4O	$R\bar{3}$	-1.271
ZrO_2	$P2_1/c$	-3.928
Li_2O_2	$P6_3/mmc$	-1.670
LiO_8	Cm	-0.426
Li_3LaO_3	$Pm\bar{3}m$	-2.634
$La_2Zr_2O_7$	$Fd\bar{3}m$	-3.987
Li_2ZrO_3	$C2/c$	-3.118
$La_4Ga_2O_9$	$P2_1/c$	-3.419
$La_3Ga_5O_{12}$	$Ia\bar{3}d$	-2.927
$LiGa_5O_8$	$P4_332$	-2.310
$LiGaO_2$	$Pna2_1$	-2.388
Li_5GaO_4	Pbca	-2.244
Ga_2O_3	C2/m	-2.262
ZrGa	$I4_1/amd$	-0.633
Zr_2Ga_3	Fdd2	-0.614
Zr_2Ga	I4/mcm	-0.470
Zr_3Ga_2	P4/mbm	-0.547
$ZrGa_3$	I4/mmm	-0.489
Zr_3Ga_5	Cmcm	-0.601
La_5Ga_3	P4/ncc	-0.481
LaGa	Cmcm	-0.601
$LaGa_2$	P6/mmm	-0.709
$LaGa_6$	P4/nbm	-0.367
Li_5Ga_4	$P\bar{3}m1$	-0.340

Li_2Ga_7	Cm	-0.191
LiGa	$Fd\bar{3}m$	-0.330
Li_2Ga	Cmcm	-0.306
Li_3Ga_2	$R\bar{3}m$	-0.333
Li	$R\bar{3}m$	0
La	$P6_3/mmc$	0
Zr	$P6_3/mmc$	0
Ga	Cmce	0
O_2	C2/m	0

The formation enthalpies (E_f) of an A_mB_n compound, representing the energy change when a compound is formed from its constituent elements in their standard state, is calculated by $E_f[A_mB_n]=\{E[A_mB_n]-m*E[A]-n*E[B]\}/(m+n)$ with E is the total ground state energy under DFT calculation.

Table S2. Thermodynamically favorable reactions could be occured at $Li/Ga_{0.25}LLZO$ interface as shown in Figure 5(a) (LLZO is presumed to be a stable phase toward Li).

ID	Interfacial reaction equations	E_r (meV/atom)
A	$0.444\ Li_{6.25}Ga_{0.25}La_3Zr_2O_{12} + 0.556\ Li \rightarrow 0.444\ Li_7La_3Zr_2O_{12} + 0.111\ Li_2Ga$	-63.82
B	$0.45\ Li_{6.25}Ga_{0.25}La_3Zr_2O_{12} + 0.55\ Li \rightarrow 0.4\ Li_7La_3Zr_2O_{12} + 0.0875\ Li_2Ga + 0.0125\ Li_3Ga$	-63.71
C	$0.5\ Li_{6.25}Ga_{0.25}La_3Zr_2O_{12} + 0.5\ Li \rightarrow 0.5\ Li_7La_3Zr_2O_{12} + 0.5\ LiGa$	-61.85

D	$0.55\ Li_{6.25}Ga_{0.25}La_3Zr_2O_{12} + 0.45\ Li \rightarrow 0.55\ Li_7La_3Zr_2O_{12} + 0.01875\ Li_2Ga_7 + 0.00625\ Ga$	-57.93
$Ga_{0.25}$LLZO	$Li_{6.25}Ga_{0.25}La_3Zr_2O_{12} \rightarrow 0.8667\ Li_7La_3Zr_2O_{12} + 0.1833\ LiGaO_2 + 0.1333\ La_2Zr_2O_7 + 0.0333\ La_4Ga_2O_9$	-19.19

Table S3. Thermodynamically favorable reactions could be occured at Li/$Ga_{0.125}$LLZO interface as shown in Figure 5(b) (LLZO is presumed to be a stable phase toward Li).

ID	Interfacial reaction equations	E_r (meV/atom)
A'	$0.6154\ Li_{6.625}Ga_{0.125}La_3Zr_2O_{12} + 0.3846\ Li \rightarrow 0.6154\ Li_7La_3Zr_2O_{12} + 0.0769\ Li_2Ga$	-36.42
B'	$0.65\ Li_{6.625}Ga_{0.125}La_3Zr_2O_{12} + 0.35\ Li \rightarrow 0.65\ Li_7La_3Zr_2O_{12} + 0.0094\ Li_3Ga_2 + 0.0156\ Li_5Ga_4$	-35.85
C'	$0.7\ Li_{6.625}Ga_{0.125}La_3Zr_2O_{12} + 0.3\ Li \rightarrow 0.7\ Li_7La_3Zr_2O_{12} + 0.0175\ LiGa + 0.01\ Li_2Ga_7$	-33.67
$Ga_{0.125}$LLZO	$Li_{6.625}Ga_{0.125}La_3Zr_2O_{12} \rightarrow 0.9333\ Li_7La_3Zr_2O_{12} + 0.0917LiGaO_2 + 0.0667\ La_2Zr_2O_7 + 0.0167\ La_4Ga_2O_9$	-14.02

Supplementary movie S1 and S2 are also available.

Movie S1 shows the real time reducing reaction of $Li_{6.4}Ga_{0.2}La_3Zr_2O_{12}$ when placing it onto a 250 °C heating plate.

Movie S2 shows the real time reaction of $LiGaO_2$ when placing it onto a 250 °C heating plate.